Asymmetric pendulum effect and transparency change of $\mathcal{PT}$-symmetric photonic crystals under dynamical Bragg diffraction beyond the paraxial approximation

V. A. Bushuev, L. V. Dergacheva, and B. I. Mantsyzov*
Department of Physics, Moscow State University, Moscow 119991, Russia
(Received 26 September 2016; published 31 March 2017)

Light propagating in $\mathcal{PT}$-symmetric photonic crystals (PhCs) under Bragg diffraction in the Laue geometry has been studied theoretically using the spectral method. The $\mathcal{PT}$-symmetric solutions describing propagating modes have been found in the PhCs with gain and loss beyond paraxial approximation. We described the pendulum effect—the periodical spatial localization of the total field intensity in a PhC—near the $\mathcal{PT}$-symmetry-breaking point. It is shown that, due to $\mathcal{PT}$-symmetric properties of the medium, an asymmetric change in the amplitudes of the diffracted waves in PhCs is observed when the sign of the Bragg incidence angle is changed from positive to negative. Thus, the intensity of a spatially periodic field in a medium radically alters under the pendulum effect. Moreover, when the sign of the Bragg incidence angle changes, a PhC of a certain thickness is turned from an absorbing structure into an amplifying one, also a PhC of any thickness evolves from completely transparent into amplifying in the vicinity of the $\mathcal{PT}$-symmetry-breaking point. Under a small change of the imaginary part of permittivity, the light switching from a transmitted wave into a gain or loss diffracted wave is possible in a diffraction-thick PhC.

DOI: 10.1103/PhysRevA.95.033843

I. INTRODUCTION

Photonic crystals have been studied actively for quite a long period in order to detect novel optical phenomena [1–3] as well as to be able to use them for effectively managing light beams and pulses [4,5] and transformation of light parameters [6,7]. When analyzing dynamical light diffraction in the Laue geometry "on transmission" [8,9], the diffraction-induced splitting of femtosecond laser pulses [10–12], selective compression [13,14], as well as the pendulum effect have been revealed [15–18]. The pendulum effect is associated with a beating of eigenmodes in PhCs. This involves a periodical energy exchange between the transmitted and the diffracted waves and, as a consequence, an opportunity to switch the output radiation from the transmitted wave to the diffracted one when changing medium parameters or light parameters. These effects were examined in detail theoretically and experimentally in conservative [15–18] and absorbing media (the Borrmann effect) [19].

In recent years a novel direction of optical research is being developed—optics of parity-time-symmetric ($\mathcal{PT}$-symmetric) media [20,21]. The similarity between the quantum-mechanical Schrödinger equation for the complex potential and the wave equation for the electric field in the medium possessing complex permittivity, i.e., in the medium with absorption and amplification, enabled extrapolating results, obtained from resolving the quantum-mechanical problems with the pseudo-Hermitian operator, to the optical problems of light propagation and scattering in nonconservative media. When the complex potential is $\mathcal{PT}$ symmetric, i.e., it is invariant under transformation by parity and time-reversal operators, the pseudo-Hermitian operator of the Schrödinger equation has real eigenvalues of energy [22,23]. In the case of the wave equation in optical problems this is equivalent to the existence of real wave numbers and the propagating mode in the medium possessing $\mathcal{PT}$-symmetric permittivity $\varepsilon(x) = \varepsilon^*(-x)$ [24,25]. The function of permittivity $\varepsilon(x) = \varepsilon'(x) + i\varepsilon''(x)$, where $\varepsilon'(x)$ and $\varepsilon''(x)$ are even and odd periodical functions, respectively, is a $\mathcal{PT}$-symmetric one. An example of these nonconservative media is periodical structures with light absorption $\varepsilon''(x) > 0$ and light amplification $\varepsilon''(x) < 0$ or $\mathcal{PT}$-symmetric photonic crystals [24–28]. Propagating $\mathcal{PT}$-symmetric modes [29], asymmetry of transmission in the case when the input and output surfaces are swapped [30,31], and spontaneous decay of $\mathcal{PT}$-symmetric modes [29] were observed in these structures. Recently, the asymmetric diffraction based on a passive $\mathcal{PT}$-symmetric diffraction grating was considered theoretically [32]. The possibility of light propagation in $\mathcal{PT}$-symmetric PhCs under Bragg diffraction in the Laue geometry has been considered previously in paraxial approximation [26,27] where the Bragg incidence angle is so small $\theta_B \ll 1$ that effects derived from spatial divergence of transmitted and diffracted waves are negligible. It was shown that $\mathcal{PT}$-symmetric PhCs are not transparent because the waves evolving inside them do not explore the gain and loss regions equally.

Here we present the solution of a boundary problem of dynamical Bragg diffraction in $\mathcal{PT}$-symmetric PhCs in the Laue geometry for the incident plane monochromatic wave and beam beyond paraxial approximation, i.e., at an arbitrary value of the Bragg incidence angle $\theta = \theta_B$ (Fig. 1). In this case dependence of the field spatial structure on medium parameters has been investigated.

The case of weak reflection from the PhC surfaces is considered to demonstrate general bulk effects most clearly. The present investigation shows that in $\mathcal{PT}$-symmetric PhC spatial distribution of total field intensity under the pendulum effect depends not only on a value of the gain-loss parameter, but also on the chosen sign of the Bragg incidence angles $\theta_B > 0$ and $\theta_B < 0$ (Fig. 1). Unlike the conservative PhC, the field intensity in the $\mathcal{PT}$-symmetric PhC under the pendulum effect varies by orders of magnitude when the

*Corresponding author: bmantsyzov@gmail.com

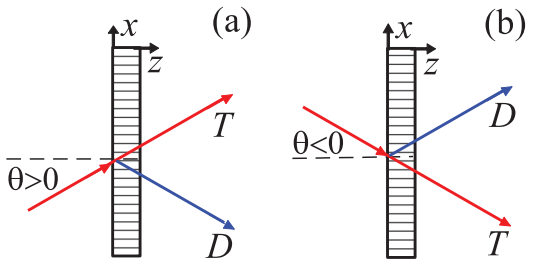

FIG. 1. Schematic of two cases of wave incidence onto the PhC: (a) $\theta > 0$ and (b) $\theta < 0$; T and D are the transmitted and diffracted waves, respectively.

sign of the incidence angle θ_B is changed from positive to negative. The $\mathcal{PT}$-symmetric PhC of a certain thickness turns from the weakly absorbing structure to the amplifying one when the angle θ_B is changed symmetrically. Such drastic changes of PhC optical properties particularly appear under dynamical diffraction near the $\mathcal{PT}$-symmetry-breaking point. If the gain-loss parameter is greater than a critical value, then $\mathcal{PT}$-symmetric eigenmodes become $\mathcal{PT}$ asymmetric, and their spatial localizations in a PhC change so that one mode is absorbed and another one grows when they propagate within the PhC.

II. DYNAMICAL DIFFRACTION IN THE LAUE SCHEME IN $\mathcal{PT}$-SYMMETRIC PHOTONIC CRYSTALS BEYOND THE PARAXIAL APPROXIMATION

Let us consider a $\mathcal{PT}$-symmetric one-dimensional PhC with harmonic modulation of permittivity,

$$\varepsilon(x) = \varepsilon_0' + \varepsilon_r \cos(hx) + i\varepsilon_i \sin(hx), \tag{1}$$

where $h = 2\pi/d$ is the module of a reciprocal lattice vector, d is the lattice period, and ε_0', ε_r, and ε_i are real values $\varepsilon_0' - |\varepsilon_r| > 1$. Suppose the plane monochromatic TE-wave $E_{\text{in}}(\mathbf{r},t) = A_{\text{in}} \exp(i\mathbf{k}\cdot\mathbf{r} - i\omega t)$ is incident onto the surface of a PhC $z = 0$ at an angle θ to the normal to its surface. Here $\mathbf{k} = (k_x, k_z)$ is the wave vector in a vacuum, $k = \omega/c = 2\pi/\lambda$, ω is the frequency of the wave, c is the speed of light in a vacuum, λ is the wavelength, and $k_x = k \sin\theta, k_z = k \cos\theta$.

The complex field $E(\mathbf{r},t) = E(\mathbf{r})\exp(-i\omega t)$ in the PhC is defined by the equation,

$$\Delta E(\mathbf{r},t) - \frac{\varepsilon(x)}{c^2}\frac{\partial^2 E(\mathbf{r},t)}{\partial t^2} = 0, \tag{2}$$

where $\Delta = \partial^2/\partial x^2 + \partial^2/\partial z^2$ is the Laplacian. Near the Bragg condition $2k \sin\theta_B = h$, it is possible to use the two-wave approximation and to represent the field in the structure as a superposition of two strong diffraction-connected waves (Fig. 1) [13],

$$E(\mathbf{r}) = A_0 \exp(i\mathbf{q}_0\cdot\mathbf{r}) + A_h \exp(i\mathbf{q}_h\cdot\mathbf{r}), \tag{3}$$

where $A_{0,h}$ are amplitudes of the transmitted (T) and diffracted (D) waves, respectively; $\mathbf{q} = (q_{0x}, q_{0z})$, $\mathbf{q}_h = (q_{hx}, q_{hz})$ are wave vectors of the transmitted and diffracted waves in the PhC; $q_{hx} = q_{0x} - h$, $q_{0z} = q_{hz}$. By substituting into Eq. (2) the expression (3) and the Fourier series expansion in the reciprocal lattice vectors of the function,

$$\varepsilon(x) = \sum_{m=-\infty}^{\infty} \varepsilon_m \exp(-imhx),$$

where the Fourier coefficients are

$$\varepsilon_m = \frac{1}{d}\int_0^d \varepsilon(x)\exp(imhx)dx, \tag{4}$$

we obtain the following equations for the field amplitudes:

$$\left(\varepsilon_0 k^2 - q_{0x}^2 - q_{0z}^2\right)A_0 + \varepsilon_{-1}k^2 A_h = 0, \tag{5a}$$

$$\varepsilon_1 k^2 A_0 + \left[\varepsilon_0 k^2 - (q_{0x} - h)^2 - q_{0z}^2\right]A_h = 0, \tag{5b}$$

where $q_{0x} = k_x$, which follows from the boundary conditions. The existence condition of nontrivial solutions of the system of Eqs. (5) allows us to write down dispersion relations for z projections of the wave vectors of the transmitted and diffracted waves of two eigenmodes, called the Borrmann $q_{0z}^{(1)}$ and anti-Borrmann $q_{0z}^{(2)}$ modes,

$$\left(q_{0z}^{(1,2)}\right)^2 = \varepsilon_0 k^2 - q_{0x}^2 + \alpha_0 h \mp \left(\alpha_0^2 h^2 + \varepsilon_1\varepsilon_{-1}k^4\right)^{1/2}, \tag{6}$$

where $\alpha_0 = q_{0x} - h/2$ defines the degree of detuning from the exact Bragg condition $q_{0x} = h/2$. Dispersion relations for the diffracted waves are obtained by the replacement $q_{0x} = q_{hx} + h$, $q_{0z}^{(1,2)} = q_{hz}^{(1,2)}$ in Eq. (6). Equation (5a) provides the following relations for the field amplitudes:

$$A_{hj} = R_j A_{0j},$$

$$R_{1,2} = \left[\alpha_0 h \mp \left(\alpha_0^2 h^2 + \varepsilon_1\varepsilon_{-1}k^4\right)^{1/2}\right]\Big/\varepsilon_{-1}k^2, \tag{7}$$

where R_j's are the partial amplitude coefficients of the diffraction reflection of the waves and A_{0j}, A_{hj} are amplitudes of the Borrmann ($j = 1$) and anti-Borrmann ($j = 2$) modes.

Exact expressions for amplitudes of the reflected waves A_1 and A_2 with x projections of the wave-vectors $k_{1x} = k_x$ and $k_{2x} = k_x - h$ in a vacuum ($z < 0$) and $A_{0j}, A_{hj} (z > 0)$ in the PhC are obtained from continuity conditions for the electric and magnetic fields at the boundaries of the PhC. The calculations show that these amplitudes are negligibly small with the PhC parameters used below: $A_1 \leqslant 0.07A_{\text{in}}$, $A_2 \leqslant 0.02A_{\text{in}}$. Besides, in the case of a semi-infinite PhC we will neglect backward waves with $q_{0z}^{(1,2)} < 0$. Therefore for simplicity and clarity let us consider the case of weak mirror light reflection from the PhC boundaries. Then, supposing $A_{\text{in}} = 1$ and neglecting amplitudes of the reflected fields, the following expressions for amplitudes of the transmitted waves A_{01} and A_{02} are obtained easily from the boundary conditions $A_{01} + A_{02} = 1$ and $A_{h1} + A_{h2} = 0$:

$$A_{01} = -R_2/(R_1 - R_2), \quad A_{02} = R_1/(R_1 - R_2). \tag{8}$$

In the exact Bragg condition $\alpha_0 = 0$ the coefficients of diffraction reflection in Eqs. (7) and (8) are

$$R_{1,2} = \mp\sqrt{\varepsilon_1\varepsilon_{-1}}/\varepsilon_{-1}. \tag{9}$$

In a general case of the complex function $\varepsilon(x)$, the Fourier coefficients $\varepsilon_{\pm1}$ are complex as well, and there are no propagating (undamped) modes due to the complex z projections $q_{0z}^{(1,2)}$ in Eq. (6). But in the case of $\mathcal{PT}$-symmetric

media, the values of $\varepsilon_{\pm 1}$ are real. This causes the formation of propagating modes. Indeed, it appears from Eqs. (1) and (4) that

$$\varepsilon_0 = \varepsilon_0', \quad \varepsilon_1 = (\varepsilon_r - \varepsilon_i)/2, \quad \varepsilon_{-1} = (\varepsilon_r + \varepsilon_i)/2, \tag{10}$$

so $\sqrt{\varepsilon_1\varepsilon_{-1}} = \sqrt{\varepsilon_r^2 - \varepsilon_i^2}/2$. Hence, propagating modes Eq. (6) exist when $|\varepsilon_i| < |\varepsilon_r|$, and they are $\mathcal{PT}$ symmetric. In the singular point $|\varepsilon_i| = |\varepsilon_r|$, so-called $\mathcal{PT}$-symmetry breaking takes place, and above the singular point $|\varepsilon_i| > |\varepsilon_r|$, there exist gain and loss $\mathcal{PT}$-asymmetric modes in the structure.

III. ASYMMETRY OF THE PENDULUM EFFECT IN $\mathcal{PT}$-SYMMETRIC PHOTONIC CRYSTALS UNDER A CHANGING SIGN OF THE BRAGG INCIDENCE ANGLE

Consider magnitudes and spatial distribution of the field amplitudes in the PhCs in these three cases: $|\varepsilon_i| < |\varepsilon_r|$, $|\varepsilon_i| = |\varepsilon_r|$, and $|\varepsilon_i| > |\varepsilon_r|$. The wave amplitudes Eqs. (7) and (8) in the exact Bragg condition are defined by the reflection coefficients Eq. (9),

$$R_{1,2} = \mp\sqrt{(\varepsilon_r - \varepsilon_i)/(\varepsilon_r + \varepsilon_i)}. \tag{11}$$

Since Eq. (11) provides $R_1 - R_2 = -2[(\varepsilon_r - \varepsilon_i)/(\varepsilon_r + \varepsilon_i)]^{1/2}$, then amplitudes of the transmitted waves Eq. (8) under the exact Bragg condition are equal to each other: $A_{01} = A_{02} = 1/2$ and do not depend on magnitudes ε_r and ε_i. On the contrary, amplitudes of the diffracted waves in Eq. (7) depend on the relation between ε_r and ε_i in Eq. (11): $A_{h1} = -A_{h2} = R_1/2$. To be specific we assume $\varepsilon_r > 0$ and $\varepsilon_i > 0$. The total fields of the transmitted E_0 and diffracted E_h waves below the singularity $\varepsilon_i < \varepsilon_r$,

$$E_0(x,z) = \left[A_{01}\exp\left(iq_{0z}^{(1)}z\right) + A_{02}\exp\left(iq_{0z}^{(2)}z\right)\right]\exp(iq_{0x}x), \tag{12a}$$

$$E_h(x,z) = \left[A_{h1}\exp\left(iq_{0z}^{(1)}z\right) + A_{h2}\exp\left(iq_{0z}^{(2)}z\right)\right] \times \exp[i(q_{0x} - h)x] \tag{12b}$$

oscillate along the z axis in the PhC with the period $2\Lambda_{\rm ex}$ due to the superposition of the Borrmann and anti-Borrmann modes with the difference of z projections of the wave-vectors $q_{0z}^{(2)} - q_{0z}^{(1)} = \pi/\Lambda_{\rm ex}$. Here $\Lambda_{\rm ex}$ is the extinction depth, i.e., the distance in the PhC where the transmitted wave vanishes due to the total energy transfer into the diffracted wave and vice versa (Fig. 2). If modulation is weak, i.e., when $\varepsilon_{r,i} \ll 1$,

$$\Lambda_{\rm ex} = \lambda\sqrt{\varepsilon_0 - \sin^2\theta}/2\sqrt{\varepsilon_1\varepsilon_{-1}} = \lambda\sqrt{\varepsilon_0 - \sin^2\theta}/\sqrt{\varepsilon_r^2 - \varepsilon_i^2}. \tag{13}$$

Figure 2 represents dependencies of intensities of the transmitted $I_0(z) = |E_0|^2$ (12a) and diffracted $I_h(z) = |E_h|^2$ (12b) waves on the depth z in the PhC for two different values of the imaginary part of dielectric permittivity ε_i.

Curves 1 and 2 in Fig. 2(a) indicate the typical picture of the pendulum oscillations under traditional diffraction in the Laue geometry in the conservative PhC, i.e., with $\varepsilon_i = 0$. In this case $R_{1,2} = \mp 1$ [see Eq. (11)] and $\Lambda_{\rm ex0} \equiv \Lambda_{\rm ex}(\varepsilon_i = 0) = 7.8\,\mu$m. Intensities of the transmitted and diffracted waves vary from

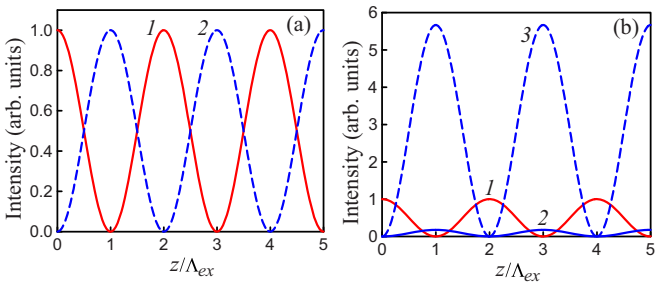

FIG. 2. (a) The dependence of intensities of the transmitted $I_0(z)$ (curve 1) and diffracted $I_h(z)$ (dashed curve 2) waves on the depth z in a conservative PhC when $\varepsilon_i = 0$ and $\theta = \theta_B$. (b) The intensities of transmitted $I_0(z)$ (curve 1) and diffracted $I_h(z)$ (curve 2) waves when $\theta_B > 0$ and $I_h(z)$ when $\theta_B < 0$ (dashed curve 3) in the case of a $\mathcal{PT}$-symmetric PhC with $\varepsilon_i = 0.07$. The parameters are $d = 800$ nm, $\lambda = 800$ nm, $\theta_B = \pm 30^\circ$, $\varepsilon_0 = 1.2$, and $\varepsilon_r = 0.1$.

0 to 1. When $\theta_B > 0$, in the $\mathcal{PT}$-symmetric photonic crystal with $\varepsilon_i = 0.07$, the intensity of the transmitted wave $I_0(z)$ does not change [curves 1, Figs. 2(a) and 2(b)], and the intensity of the diffracted wave $I_h(z)$ sharply decreases [curve 2, Fig. 2(b)] because $|R_{1,2}| < 1$ and the extinction depth $\Lambda_{\rm ex} = 10.9\,\mu$m increases. Thereby at $\theta = \theta_B$ the $\mathcal{PT}$-symmetric PhC with the thickness $L = 2m\Lambda_{\rm ex}$, where m is an integer, is completely transparent, i.e., $I_0(L) = 1$, and the PhC with $L = (2m + 1)\Lambda_{\rm ex}$ absorbs and scatters radiation into the direction of the diffracted wave [$I_h(L) < 1$, $I_0(L) = 0$].

When ε_i approaches ε_r ($\varepsilon_i \to \varepsilon_r$) the reflection coefficients Eq. (11) decrease. The coefficients $R_{1,2}$ and the intensity of the diffracted wave $I_h(z)$, respectively, decrease and vanish when $\varepsilon_i = \varepsilon_r$ [Fig. 3(a), curve 2]. Radiation in the PhC becomes one mode because $q_{0z}^{(1)} = q_{0z}^{(2)} = k(\varepsilon_0 - \sin^2\theta_B)^{1/2}$ in Eq. (12). At the same time the intensity of the transmitted wave $I_0(z)$ tends to 1 at any finite value of the depth z [Fig. 3(a), curve 1], and the extinction depth $\Lambda_{\rm ex}$ Eq. (13) formally approaches infinity. Accordingly, the $\mathcal{PT}$-symmetric PC becomes completely transparent at $\theta_B > 0$, i.e., $I_0(L) = 1$ and $I_h(z) = 0$, irrespective of its thickness.

The symmetric sign change of the Bragg incidence angle $\theta_B > 0 \to \theta_B < 0$ causes a radical change of the dynamical diffraction pattern in the $\mathcal{PT}$-symmetric PhC. Indeed, changing projection of the wave vector at the boundary of the PhC

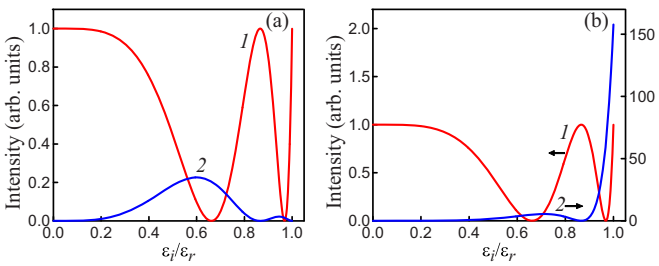

FIG. 3. The dependence of intensities of the transmitted I_0 (curve 1) and diffracted I_h (curve 2) waves on the relation $\varepsilon_i/\varepsilon_r$ at incidence angles (a) $\theta_B > 0$ and (b) $\theta_B < 0$. The PhC thickness is $L = 4\Lambda_{\rm ex\,0} = 31.2\,\mu$m, and the other parameters are the same as in the caption for Fig. 2.

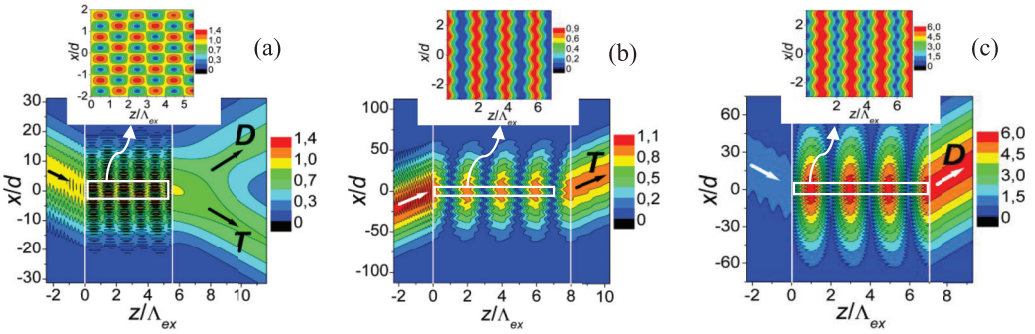

FIG. 4. Two-dimensional cards of spatial distribution of the modulus of total field $|E'(x,z)| = |E'_0(x,z) + E'_h(x,z)|$ for input ($z < 0$) and output ($z > L$) beams as well as in a PhC ($0 < z < L$) under the exact Bragg condition. The straight arrows indicate the direction of input and output beams. (a) A conservative PhC with $\varepsilon_0 = 1.3$, $\varepsilon_r = 0.2$, $\varepsilon_i = 0$, and $L = 5.5\Lambda_{ex}$. The field maximum within the PhC is $|E'|_{max} = 1.4$. (b) A $\mathcal{PT}$-symmetric PhC, $\varepsilon_i = 0.19$, $L = 8\Lambda_{ex}$, $\theta_B > 0$, and $|E'|_{max} = 0.9$. (c) A $\mathcal{PT}$-symmetric PhC, $\varepsilon_i = 0.19$, $L = 7\Lambda_{ex}$, $\theta_B < 0$, and $|E'|_{max} = 6$. The insets: The fields' distribution in the selected areas.

from $q_{hx} = q_{0x} - h$ to $q_{hx} = q_{0x} + h$ leads to the exchange of the Fourier coefficients $\varepsilon_1 \leftrightarrow \varepsilon_{-1}$ in Eqs. (5). This is equivalent to the sign change of the value ε_i. The reflection coefficients Eqs. (9) and (11) now may be written as follows:

$$R_{1,2} = \mp\sqrt{\varepsilon_1\varepsilon_{-1}}/\varepsilon_1 = \mp\sqrt{(\varepsilon_r + \varepsilon_i)/(\varepsilon_r - \varepsilon_i)}. \qquad (14)$$

Amplitudes of the diffracted waves now will increase when the magnitude ε_i approaches the singularity. The sign change of the incidence angle to the opposite sign can be obtained using a simple 180° turn of the PhC around the normal to the PhC surface.

Figure 2(b) shows that the intensity of the transmitted radiation $I_0(z)$ still oscillates between 0 and 1 (curve 1) and the intensity $I_h(z)$ significantly increases (curve 3). The PhC with the thickness $L = 2m\Lambda_{ex}$ still stays transparent, but the PhC with the thickness $L = (2m + 1)\Lambda_{ex}$ significantly enhances radiation in the direction of the diffracted wave. In the limited PhC this increase is not infinite because $\Lambda_{ex} \to \infty$ and $L < \Lambda_{ex}$ in the singularity. Thus, the symmetric change of the Bragg incidence angle $\theta_B > 0 \to \theta_B < 0$ leads to the asymmetric amplitude change of the diffracted waves. As a consequence, it leads to the change of transparency of the PhC under the pendulum effect, i.e., when $L = (2m + 1)\Lambda_{ex}$, a weak absorbing PhC begins to amplify radiation strongly in the direction of diffracted wave. In the vicinity of the singularity $\varepsilon_i \to \varepsilon_r$ a completely transparent PhC begins to amplify radiation in accordance with the quadratic law $I_h(z) = [k^2\varepsilon_r^2/4(\varepsilon_0 - \sin^2\theta_B)]z^2$ when the sign of the incidence angle is changed. This phenomenon happens independently on the structure thickness [Fig. 3(b)]. As is seen from Fig. 3(a), for a fixed thickness of structure L, the incident wave can be switched from the forward direction ($\varepsilon_i = 0.87\varepsilon_r$, curve 1) into the direction of the diffracted wave ($\varepsilon_i = 0.95\varepsilon_r$, curve 2) by a change in the gain-loss parameter. The diffracted wave either will be weakened [curve 2 in Fig. 3(a)] or will be enhanced [curve 2 in Fig. 3(b)], depending on the sign of incidence angle.

Similar ratios of the values of transmitted and diffracted waves' intensities also occur in the case of propagation of a monochromatic wave packet, or light beam, into a PhC. The boundary problem of the diffraction of the light beam near the Bragg condition has been solved by the spectral method [13]. The incident pulse is represented as a Fourier decomposition into plane monochromatic waves with different wave vectors. Subsequently, once the Fourier amplitudes of each of the plane waves inside the PhC and in free space have been determined in the two-wave approximation, we perform a Fourier synthesis and find the field strengths of the transmitted $[E'_0(x,z)]$ and diffracted $[E'_h(x,z)]$ beams at different points in space.

In Fig. 4, the input Gaussian beam of a unit amplitude falls on the PhC, which is localized in the region $0 < z < L$. The oscillations of the input beam field near the left boundary are caused by the interference of the incident and weak reflected waves. Obviously, if amplitudes of the diffracted field in the $\mathcal{PT}$-symmetric PhCs are changed nearby the $\mathcal{PT}$-symmetry-breaking point, this leads to an efficient change of the spatial localization of total field in the crystal $|E'(x,z)| = |E'_0(x,z) + E'_h(x,z)|$ (see Fig. 4), i.e., to the change of the field structure under the pendulum effect compared with the case of the conservative PhC [Fig. 4(a)]. In the first case reviewed above ($\theta_B > 0$) the condition $|E'_0| \gg |E'_h|$ is fulfilled, thus the field structure is defined mainly by the superposition of the transmitted waves and $|E'|_{max} \approx 1$ in Fig. 4(b). In the second case ($\theta_B < 0$) the PhC is an amplifying structure $|E'_0| \ll |E'_h|$, and the spatial structure of the total field in the medium is defined by the diffracted waves. The field maxima in the interference pattern increase significantly $|E'|_{max} \approx 6$ [Fig. 4(c)]. The fields of output beams for the conservative PhC [Fig. 4(a)] and for the $\mathcal{PT}$-symmetric crystal at $\theta_B > 0$ [Fig. 4(b)] have the values commensurate with the field of the input beam. When the sign of the incidence angle θ_B is changed from positive to negative, the diffracted output beam is amplified significantly [Fig. 4(c)].

Above we have considered an incident wave at the exact Bragg angle. It is interesting to analyze angular dependencies of the intensities $I_0(\Delta\theta)$ and $I_h(\Delta\theta)$ as the functions of detuning from the Bragg angle $\Delta\theta = \theta - \theta_B$ when PhC thickness is fixed. From the expressions (6) and (7) it follows that the region of strong diffraction reflection is defined by the condition $|\alpha_0| \leqslant k^2\sqrt{\varepsilon_1\varepsilon_{-1}}/h$. Hence, we obtain that the total effective width of the Bragg reflection is defined by the expression $\Delta\theta_B = (\varepsilon_r^2 - \varepsilon_i^2)^{1/2}/\sin 2\theta_B$.

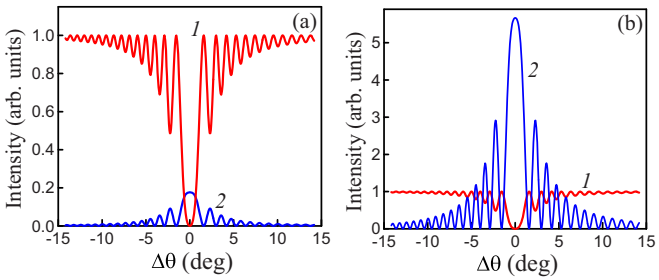

FIG. 5. The dependence of intensities of the transmitted $I_0(\Delta\theta)$ (curves 1) and diffracted $I_h(\Delta\theta)$ (curves 2) waves on the detuning $\Delta\theta = \theta - \theta_B$ from the Bragg angle at the PhC thickness $L = 5\Lambda_{ex} = 56.6\,\mu$m and $\varepsilon_i = 0.07$ if (a) $\theta > 0$ and (b) $\theta < 0$; the angular width is $\Delta\theta_B = 4.7^\circ$. The parameters are the same as in Fig. 2.

When $\varepsilon_i \to \varepsilon_r$, the width $\Delta\theta_B$ decreases and vanishes in the singularity. Figure 5 illustrates curves of diffraction transmission and reflection [angular dependencies of the intensities $I_0(\Delta\theta)$ and $I_h(\Delta\theta)$] at positive and negative incidence angle θ. It is seen that the transmission curve $I_0(\Delta\theta)$ does not depend on a sign of angle θ [curves 1 in panels (a) and (b)]. The diffraction reflection curve $I_h(\Delta\theta)$ significantly increases at the sign change of θ [curve 2 in Fig. 5(b)]. When the thickness of the PhC increases, the period of inner oscillations at the curves' edges decreases.

Larger values $m = L/2\Lambda_{ex} \gg 1$ are typical for diffraction-thick PhCs [18]. Thus, the output radiation can be switched from the forward direction with intensity $I_0(L)$ into the diffraction one with $I_h(L)$ through a small change of the extinction depth Λ_{ex} [Eq. (13)] at a small variation of the gain-loss parameter. For example, a transparent (I_0=1, I_h=0) $\mathcal{PT}$-symmetric PhC can be transformed into an absorbing one ($I_0 = 0$, $I_h \ll 1$) by small changing $\Delta\varepsilon_i \sim 10^{-3}$ at $\theta_B > 0$ or into an amplifying crystal ($I_0 = 0$, $I_h \gg 1$) at $\theta_B < 0$.

Below the singularity $\varepsilon_i < \varepsilon_r$ the Borrmann and anti-Borrmann eigenmodes,

$$E_1(x,z) = \{A_{01}\exp(iq_{0x}x) + A_{h1}\exp[i(q_{0x} - h)x]\} \times \exp\left(iq_{0z}^{(1)}z\right), \tag{15a}$$

$$E_2(x,z) = \{A_{02}\exp(iq_{0x}x) + A_{h2}\exp[i(q_{0x} - h)x]\} \times \exp\left(iq_{0z}^{(2)}z\right) \tag{15b}$$

are propagating $\mathcal{PT}$-symmetric modes because $q_{0z}^{(1,2)}$ (6) are real functions. Therefore, their intensities $I_{1,2}(x) = |E_{1,2}(x,z)|^2$ do not depend on z. In crossing the singularity $\varepsilon_i > \varepsilon_r$, the complex values $q_{0z}^{(1,2)}$ (6) in Eqs. (15) lead to a gain or loss of these modes, and the solutions (15) become $\mathcal{PT}$ asymmetric. The corresponding intensities increase or decrease exponentially with the depth z: $I_{1,2}(x,z) \propto \exp(\pm\mu z)$. From the relations (6) and (15) it follows that the gain-loss coefficient is

$$\mu = \pi\sqrt{\varepsilon_i^2 - \varepsilon_r^2}/\lambda\sqrt{\varepsilon_0 - \sin^2\theta_B}. \tag{16}$$

In Fig. 6 it clearly is seen how spatial localization of the Borrmann and anti-Borrmann modes changes in crossing the $\mathcal{PT}$-symmetry-breaking point.

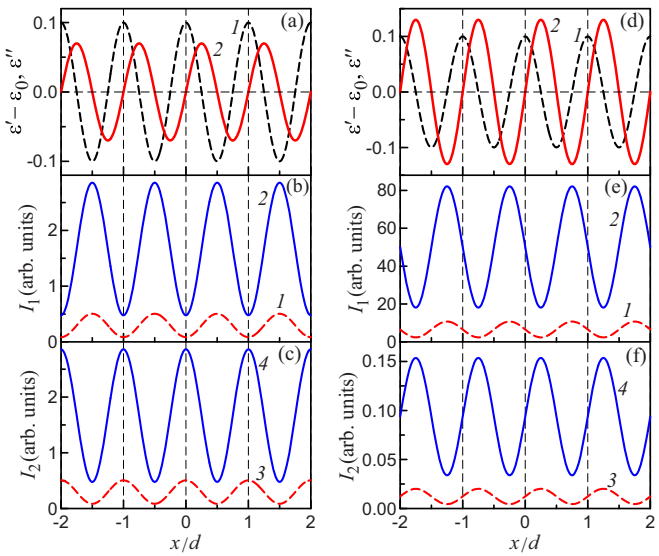

FIG. 6. (a) Spatial distribution of the real (curve 1) and imaginary (curve 2) parts of the permittivity $\varepsilon(x)$ for a $\mathcal{PT}$-symmetric PhC with $\varepsilon_i = 0.07 < \varepsilon_r = 0.1$. (b) Distributions of the Borrmann $\mathcal{PT}$-symmetric mode $I_1(x,L)$ (curves 1 and 2) and (c) the anti-Borrmann $\mathcal{PT}$-symmetric mode $I_2(x,L)$ (curves 3 and 4) along the x axis in the PhC at incidence angles $\theta_B > 0$ (dashed curves 1 and 3) and $\theta_B < 0$ (curves 2 and 4). (d) Spatial distribution of the real (curve 1) and imaginary (curve 2) parts of the permittivity $\varepsilon(x)$ for a $\mathcal{PT}$-asymmetric PhC with $\varepsilon_i = 0.13 > \varepsilon_r = 0.1$. (e) Distributions of the Borrmann mode $I_1(x,L)$ (curves 1 and 2) and (f) of the anti-Borrmann mode $I_2(x,L)$ (curves 3 and 4) along the x axis in the PhC at incidence angles $\theta_B > 0$ (dashed curves 1 and 3) and $\theta_B < 0$ (curves 2 and 4). The length of the structure is $L = \pi/\mu = 9.4\,\mu$m, and the other parameters are the same as in Fig. 2.

Figure 6(b) shows that the Borrmann intensities $I_1(x)$ are localized, i.e., maximal, among the planes $x = 0, \pm d, \pm 2d$, and so on, whereas the anti-Borrmann intensities $I_2(x)$ are localized on these planes [Fig. 6(c)]. At the same time when the sign of the incidence angle is changed, intensities $I_{1,2}(x)$ increase significantly [curves 2 in Fig. 6(b) and 4 in Fig. 6(c)]. This is caused by an increase in amplitudes $A_{h1,h2}$ in Eqs. (15) due to an increase in reflection coefficients $R_{1,2}$ Eq. (14). When one compares curves in Figs. 6(b) and 6(c) with the distribution of the imaginary part of the permittivity in Fig. 6(a) (curve 2), it is clear that the $\mathcal{PT}$-symmetric modes are localized in those regions of the PhC where both light absorption [$\varepsilon''(x) > 0$] and amplification [$\varepsilon''(x) < 0$] act simultaneously.

In crossing the $\mathcal{PT}$-symmetry-breaking point ($\varepsilon_i > \varepsilon_r$) the reflection coefficients $R_{1,2}$ become purely imaginary. At the incidence angle $\theta_B > 0$ from Eq. (9) it follows that $R_{1,2} = \mp i[(\varepsilon_i - \varepsilon_r)/(\varepsilon_i + \varepsilon_r)]^{1/2}$, whereas $|R_{1,2}| < 1$. When the sign of the incidence angle changes to $\theta_B < 0$ from Eq. (9), we obtain that $R_{1,2} = \pm i[(\varepsilon_i + \varepsilon_r)/(\varepsilon_i - \varepsilon_r)]^{1/2}$. It means that the absolute values of the reflection coefficients are $|R_{1,2}| > 1$. The presence of the imaginary unit in the second terms in Eqs. (15) leads to displacement of the spatial distributions of the $\mathcal{PT}$-asymmetric Borrmann [Fig. 6(e)] and anti-Borrmann [Fig. 6(f)] modes by the value of $d/4$ along the x axis compared to curves in Figs. 6(b) and 6(c). It is worth

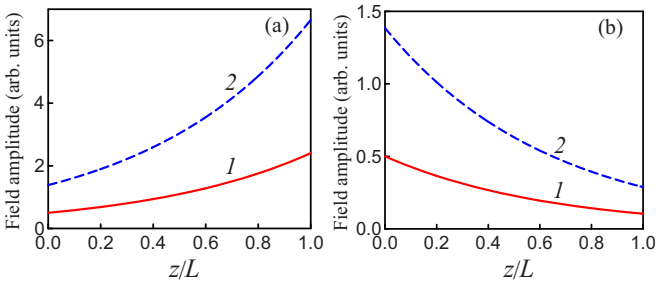

FIG. 7. The dependence of the absolute values of the $\mathcal{PT}$-asymmetric (a) Borrmann fields E_{10} (curve 1) and E_{1h} (dashed curve 2) and (b) anti-Borrmann fields E_{20} (curve 1) and E_{2h} (dashed curve 2) on the depth z in the PhC at the following parameters: $\varepsilon_r = 0.1$, $\varepsilon_i = 0.13$, $\theta_B < 0$, and $L = \pi/\mu = 9.4\,\mu$m. The other parameters are the same as in Fig. 2.

mentioning here that in these regions of the PhC the imaginary part of the permittivity is negative [curve 2 in Fig. 6(d)], thus the Borrmann mode $I_1(x,L)$ increases [Fig. 6(e)]. On the contrary, in the region where the anti-Borrmann mode $I_2(x,L)$ is localized, the imaginary part $\varepsilon''(x)$ is positive [curve 2 in Fig. 6(d)]. That leads to its loss [Fig. 6(f)].

To illustrate the foregoing, let us represent the Borrmann and anti-Borrmann modes Eq. (15) as the sum of partially transmitted and diffracted waves, belonging to different branches of the dispersion relation Eq. (6): $E_1 = E_{10} + E_{1h}$, $E_2 = E_{20} + E_{2h}$. Figure 7 shows how fields of the Borrmann mode $E_{10,1h}$ increase [Fig. 7(a)] and how fields of the anti-Borrmann mode decay [Fig. 7(b)] while they are propagating inside the PhC. For certainty we consider the case of negative incidence angle $\theta_B < 0$.

IV. CONCLUSIONS

We have described dynamical Bragg diffraction of plane monochromatic waves and beams in the $\mathcal{PT}$-symmetric PhC in the Laue geometry beyond paraxial approximation. It is demonstrated that optical properties of the $\mathcal{PT}$-symmetric PhC radically vary when the sign of the Bragg incidence angle is changed. This leads to the transformation of the absorbing PhC into a strongly amplifying one below the $\mathcal{PT}$-symmetry-breaking point $\varepsilon_i < \varepsilon_r$ at the fixed structure thickness. In these circumstances, the output intensity of the transmitted wave is zero, and only the diffracted wave is absorbed or amplified. In the vicinity of the singularity $\varepsilon_i \to \varepsilon_r$ the PhC turns from the completely transparent structure into an amplifying one at any thickness of the structure when the sign of the Bragg incidence angle is changed. In a diffraction-thick $\mathcal{PT}$-symmetric PhC, input radiation can be switched from the transmitted wave into the amplified diffracted wave by a small changing of the loss-gain parameter $\Delta\varepsilon_i \sim 10^{-3}$. Increasing intensity of the interference maxima of the pendulum effect can also be useful for enhancement of the efficiency of quasi-phase-matching generation of optical harmonics. The generation efficiency is enhanced due to an increase in electroinduced second-order nonlinearity in the maxima of pendulum-effect grating [33]. The change of the value ε_i and, correspondingly, magnitudes of the wave vectors of propagating modes can be used in the $\mathcal{PT}$-symmetric PhC to satisfy the phase-matching condition under the generation of optical harmonics.

ACKNOWLEDGMENTS

B.I.M. is grateful to V. V. Konotop for useful discussions. This work was partially supported by the Russian Foundation for Basic Research Grant No. 14-29-07197 and by the European Commission H2020 EU Project No. 691011 SOLIRING.

[1] E. Yablonovitch, Photonic crystals, J. Mod. Opt. **41**, 173 (1994).
[2] J. D. Joannopoulos, S. G. Johnson, J. N. Winn, and R. D. Meade, *Photonic Crystals: Molding the Flow of Light* (Princeton University Press, Princeton, 2008).
[3] Y. S. Kivshar and G. P. Agrawal, *Optical Solitons: From Fibers to Photonic Crystals* (Academic Press, San Diego, 2003).
[4] M. Notomi, Manipulating light with strongly modulated photonic crystals, Rep. Prog. Phys. **73**, 096501 (2010).
[5] F. Priolo, T. Gregorkiewicz, M. Galli, and T. Krauss, Silicon nanostructures for photonics and photovoltaics, Nat. Nanotechnol. **9**, 19 (2014).
[6] J. Li, L. O'Faolain, I. Rey, and T.Krauss, Four-wave mixing in photonic crystal waveguides: Slow light enhancement and limitations, Opt. Express **19**, 4458 (2011).
[7] T. Baba, Silicon gets the green light, Nat. Photon. **3**, 190 (2009).
[8] P. St. J. Russell, Bragg Resonance of Light in Optical Superlattices, Phys. Rev. Lett. **56**, 596 (1986).
[9] B. Bruser, I. Staude, G. Freymann, M. Wegener, and U. Pietsch, Visible light Laue diffraction from woodpile photonic crystals, Appl. Opt. **51**, 6732 (2012).
[10] V. A. Bushuev, B. I. Mantsyzov, and A. A. Skorynin, Diffraction-induced laser pulse splitting in a linear photonic crystal, Phys. Rev. A **79**, 053811 (2009).
[11] S. E. Svyakhovskiy, V. O. Kompanets, A. I. Maydykovskiy, T. V. Murzina, S. V. Chekalin, A. A. Skorynin, V. A. Bushuev, and B. I. Mantsyzov, Observation of diffraction-induced laser pulse splitting in a photonic crystal, Phys. Rev. A **86**, 013843 (2012).
[12] X. Yan, L. Gao, Y. Dai, X. Yang, Y. Chen, and G. Ma, Periodical energy oscillation and pulse splitting in sinusoidal volume holographic grating, Opt. Express **22**, 18527 (2014).
[13] A. A. Skorynin, V. A. Bushuev, and B. I. Mantsyzov, Dynamical Bragg diffraction of optical pulses in photonic crystals in the Laue geometry: Diffraction-induced splitting, selective compression, and focusing of pulses, J. Exp. Theor. Phys. **115**, 56 (2012).
[14] S. E. Svyakhovskiy, A. A. Skorynin, V. A. Bushuev, S. V. Chekalin, V. O. Kompanets, A. I. Maydykovskiy, T. V. Murzina, and B. I. Mantsyzov, Experimental demonstration of selective compression of femtosecond pulses in the Laue scheme of the dynamical Bragg diffraction in 1D photonic crystals, Opt. Express **22**, 31002 (2014).

[15] V. Mocella, Negative refraction in photonic crystals: Thickness dependence and Pendellosung phenomenon, Opt. Express **13**, 1361 (2005).

[16] M. L. Calvo, P. Cheben, O. Martínez-Matos, F. del Monte, and J. A. Rodrigo, Experimental Detection of the Optical Pedellosung Efect, Phys. Rev. Lett. **97**, 084801 (2006).

[17] S. Savo, E. Di Gennaro, C. Miletto, A. Andreone, P. Dardano, L. Moretti, and V. Mocella, Pendellosung effect in photonic crystals, Opt. Express **16**, 9097 (2008).

[18] V. B. Novikov, S. E. Svyakhovskiy, A. I. Maydykovskiy, T. V. Murzina, and B. I. Mantsyzov, Optical pendulum effect in one-dimensional diffraction-thick porous silicon based photonic crystals, J. Appl. Phys. **118**, 193101 (2015).

[19] G. Borrmann, Über Extinktionsdiagramme der Röntgenstrahlen von Quarz, Phys. Z. **42**, 157 (1941).

[20] A. A. Zyablovsky, A. P. Vinogradov, A. A. Pukhov, A. V. Dorofeenko, and A. A. Lisyansky, PT-symmetry in optics, Phys.-Usp. **57**, 1063 (2014).

[21] V. V. Konotop, J. Yang, and D. A. Zezyulin, Nonlinear waves in $\mathcal{PT}$-symmetric systems, Rev. Mod. Phys. **88**, 035002 (2016).

[22] C. M. Bender and S. Boettcher, Real Spectra in Non-Hermitian Hamiltonians Having $\mathcal{PT}$ Symmetry, Phys. Rev. Lett. **80**, 5243 (1998).

[23] C. M. Bender, D. C. Brody, and H. F. Jones, Complex Extension of Quantum Mechanics, Phys. Rev. Lett. **89**, 270401 (2002).

[24] R. El-Ganainy, K. G. Makris, D. N. Christodoulides, and Z. H. Musslimani, Theory of coupled optical *PT*-symmetric structures, Opt. Lett. **32**, 2632 (2007).

[25] K. G. Makris, R. El-Ganainy, D. N. Christodoulides, and Z. H. Musslimani, Beam Dynamics in $\mathcal{PT}$ Symmetric Optical Lattices, Phys. Rev. Lett. **100**, 103904 (2008).

[26] M. V. Berry, Optical lattices with PT symmetry are not transparent, J. Phys. A: Math. Theor. **41**, 244007 (2008).

[27] S. Longhi, Spectral singularities and Bragg scattering in complex crystals, Phys. Rev. A **81**, 022102 (2010).

[28] Y. V. Kartashov, V. A. Vysloukh, V. V. Konotop, and L. Torner, Diffraction control in $\mathcal{PT}$-symmetric photonic lattices: From beam rectification to dynamic localization, Phys. Rev. A **93**, 013841 (2016).

[29] C. E. Ruter, K. G. Makris, R. El-Ganainy, D. N. Christodoulides, M. Segev, and D. Kip, Observation of parity-time symmetry in optics, Nat. Phys. **6**, 192 (2010).

[30] L. Feng, Y. Xu, W. S. Fegadolli, M. Lu, J. E. Oliveira, V. R. Almaida, Y. Chen, and A. Scherer, Experimental demonstration of a unidirectional reflectionless parity-time metamaterial at optical frequencies, Nat. Mater. **12**, 108 (2012).

[31] A. Regensburger, C. Bersch, M. Miri, G. Onishchukov, D. N. Christodoulides, and U. Perschel, Parity-time symmetric photonic lattices, Nature (London) **488**, 167 (2012).

[32] X.-Y. Zhu, Y.-L. Xu, Y. Zou, X.-C. Sun, C. He, M.-H. Lu, X.-P. Liu, and Y.-F. Chen, Asymmetric diffraction based on a passive parity-time grating, Appl. Phys. Lett. **109**, 111101 (2016).

[33] D. A. Kopylov, S. E. Svyakhovskiy, L. V. Dergacheva, V. A. Bushuev, B. I. Mantsyzov, and T. V. Murzina, Observation of optical second-harmonic generation in porous-silicon-based photonic crystals in the Laue diffraction scheme, Phys. Rev. A **93**, 053840 (2016).